Magneto-transport properties in perpendicularly magnetized magnetic tunnel junctions using an $Mg_{40}Fe_{10}O_{50}$ tunnel barrier

Tatsuya Yamamoto*, Tomohiro Ichinose, Jun Uzuhashi, Takayuki Nozaki, Tadakatsu Ohkubo, Kay Yakushiji, Shingo Tamaru, Hitoshi Kubota, Shinji Yuasa

National Institute of Advanced Industrial Science and Technology (AIST), Research Center for Emerging Computing Technologies, Tsukuba, Ibaraki 305-8568, Japan

National Institute for Materials Science (NIMS), Tsukuba, Ibaraki 305-0047, Japan

Abstract

We develop perpendicularly magnetized magnetic tunnel junctions (MTJs) consisting of a CoFeB/$Mg_{40}Fe_{10}O_{50}$ (MgFeO)/CoFeB multilayer. The use of MgFeO yields a substantial improvement in the flatness of the MTJ film stack compared with conventional MTJ films using MgO as a tunnel barrier layer, and a 1.7 times enhancement in the perpendicular magnetic anisotropy energy is obtained for the ultrathin CoFeB layer deposited on the MgFeO layer. Nanostructural analysis combined with elemental distribution mapping reveals the formation of highly (001)-oriented MgFeO in the as-deposited MTJ film, and the crystalline MgFeO layer effectively inhibits diffusion of B atoms from the CoFeB layers through the tunnel barrier layer during the post-annealing process. Accordingly, the MgFeO-MTJ exhibits exceptional stability against high temperature annealing, and a large tunnel magnetoresistance ratio of 235% is demonstrated in MTJ nanopillar devices after annealing at 400°C. Ferromagnetic resonance measurements also reveal a reduced magnetic damping in the MgFeO-MTJs owing to the improved uniformity in the CoFeB layer. The present experimental results will facilitate the development of magnetoresistive

*Corresponding author
Email address: yamamoto-t@aist.go.jp (Tatsuya Yamamoto)

memory devices with increasing memory density and higher energy efficiencies.

Keywords: perpendicular magnetic anisotropy, magnetic tunnel junction, magnetoresistive random access memory

1. Introduction

Magnetic tunnel junctions (MTJs) consisting of a ferromagnetic layer/tunnel barrier/ferromagnetic layer junction are fundamental elements in the field of spintronics. The discoveries of large tunnel magnetoresistance (TMR) [1, 2, 3, 4, 5, 6, 7, 8] and large perpendicular magnetic anisotropy (PMA) in CoFe(B)/MgO/CoFe(B) junctions [9, 6, 8, 10, 11, 12] have led to the rapid development of magnetoresistive random access memory (MRAM) devices [13, 7, 14, 15, 16]. In the MRAM cell, binary data are stored in one of the ferromagnetic layers (called the free layer) in the MTJ by electrically controlling the magnetization direction, while the other ferromagnetic layer possesses a fixed magnetization to serve as a "reference" for the magnetization direction of the free layer [17]. To increase the memory density while reducing the energy required to switch the magnetization, a large PMA as well as a low magnetic damping are required for the free layer [13, 7, 14]. The MRAM application also requires the MTJ devices to be formable on Si substrates with a polycrystalline electrode using a mass-production-compatible thin film deposition process (e.g., magnetron sputtering) and to be tolerant of high temperature ($> 400^{\circ}$C) annealing to overcome the CMOS back-end-of-line process [15].

Several core stacking structures to fulfill the above requirements, such as a synthetic antiferromagnetic layer based on CoPt artificial superlattices [18], an Ir spacer layer exhibiting strong interlayer exchange coupling [19], and MgO/CoFeB/X/CoFeB/MgO multilayered free layer [20, 21, 22]. In particular, the stacking structure of MgO/CoFeB/X/CoFeB/MgO has been intensively studied towards improving the TMR and PMA after high temperature annealing [23, 21, 22, 24, 25, 26]. However, the use of an MgO/CoFeB/X/CoFeB/MgO free layer imposes another difficulty in preparing flat and uniformly magnetized CoFeB layers; even though

the CoFeB thin films favor an amorphous phase without crystal grains, the poor wettability of CoFeB on MgO leads to island growth of the CoFeB layer [27]. Such structural inhomogeneity in the free layer is unfavorable in terms of energy efficiency for the electrical control of magnetization since the structural inhomogeneity inevitably leads to a magnetic inhomogeneity in the free layer and thus a larger energy dissipation during the magnetization switching. The impact of structural inhomogeneity can be even more severe for MRAM devices driven by the voltage-controlled magnetic anisotropy (VCMA) effect at the MgO/CoFe(B) interface [28, 29, 30, 31, 32], in which the free layer is typically as thin as 1 nm to minimize the electric-field screening effect. A possible solution to reducing the structural inhomogeneity is to lower the substrate temperature during the deposition of the CoFeB layer. In our previous studies, we have shown that the deposition of CoFeB layers at a cryogenic substrate temperature enhances the PMA as well as TMR in the MgO/CoFeB junction while reducing the extrinsic component of magnetic damping due to magnetic inhomogeneity [33, 34]. Another solution may be to insert an ultrathin γ-Fe_2O_3 layer in between the MgO and CoFeB layers, as the ultrathin γ-Fe_2O_3 insertion layer has been demonstrated to improve the wettability of Fe on MgO without affecting the TMR ratio [35].

In this work, we develop perpendicularly magnetized MTJs using an $Mg_{40}Fe_{10}O_{50}$ (MgFeO) tunnel barrier and a CoFeB layer deposited at a cryogenic temperature. In contrast to Ref. [35], in which an MgO/γ-Fe_2O_3 bilayer is used as tunnel barrier, here we utilize the interfacial segregation of Fe atoms from a partially Fe-substituted MgO layer [36, 37] to improve the wettability of CoFeB. The use of MgFeO barrier layer substantially improves the homogeneity of free layer, which contributes to an enhanced PMA and reduces effective magnetic damping. More interestingly, the MgFeO-MTJs exhibit higher tolerance against high-temperature annealing, and a large TMR ratio of 235% is achieved after annealing at 400°C for 2h. We investigate the improved magnetic and electrical transport properties in MgFeO-MTJs through detailed magnetic measurements and nanostructural analysis for the MTJ films as well as magneto-transport

measurements on MTJ nanopillar devices.

2. Experimental

Thin films consisting of CoFeB (0.8 nm)/MgO or MgFeO (2.5 nm)/CoFeB (0.7- 1.0 nm)/Mo (0.3 nm)/CoFeB (0.6 nm)/MgO (1.0 nm) MTJ stacks were deposited on 300 mm Si wafers with a buffer layer using an ultrahigh-vacuum magnetron sputtering system (EXIM) manufactured by Tokyo Electron Ltd. The CoFeB/Mo/CoFeB multilayer acts as a free layer whose magnetization direction can be switched by a relatively small external field, whereas the bottom CoFeB layer magnetization is pinned by a CoPt/Ir-based synthetic antiferromagnet to serve as a reference layer. The MgO layer was deposited by DC sputtering of Mg followed by in-situ post oxidation using a pure O_2 gas whereas the MgFeO layer was deposited by RF sputtering from an $Mg_{40}Fe_{10}O_{50}$ target. We also fabricated MgO-MTJs in which the MgO layer is deposited by RF sputtering from an MgO target and confirmed that the fabrication process of the MgO layer does not affect the magnetic and electric transport properties of the MgO-MTJs. The resistance-area product (RA) of MTJs used in this work is around 500 ohm$\cdot\mu$m^2, which is compatible with the VCMA studies. For both MgO- and MgFeO-MTJs, the CoFeB layer on top of the tunnel barrier layer was deposited at -173°C, followed by the deposition of Mo/CoFeB bilayer at room temperature. The magnetic properties of unpatterned films were characterized by using a vibrating sample magnetometer (VSM) and a ferromagnetic resonance measurement system equipped with a network analyzer (VNA-FMR) [38]. The nanostructure and elemental distribution of the MTJ stacks were investigated by scanning transmission electron microscopy (STEM), nano-beam electron diffraction (NBD), electron energy loss spectroscopy (EELS), and energy dispersive X-ray spectroscopy (EDS) using FEI Titan G2 80-200. Thin foil specimens for the nanostructural analyses were prepared by a standard lift-out method using a focused ion beam with a scanning electron microscopy system (FEI Helios G4UX). To characterize the magneto-transport properties,

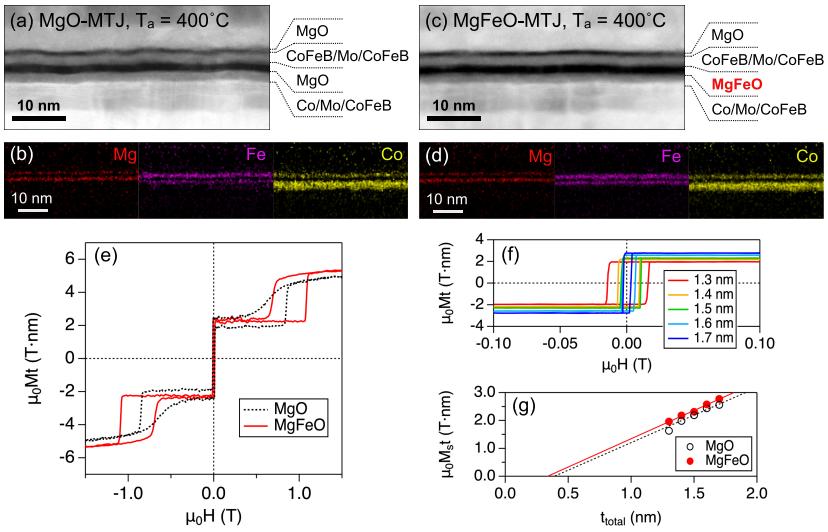

Figure 1: Layer structures and magnetic properties of MTJ films: (a,c) ADF-STEM images, (b,d) EDS elemental maps, (e) Major magnetization curves, (f) Minor magnetization curves of MgFeO-MTJ with different t_{total}, and (g) $\mu_0 M_{\mathrm{s}} t$ as a function of t_{total}. The MTJ films were annealed at $T_{\mathrm{a}} = 400^{\circ}\mathrm{C}$ for 1h after deposition. Lines in (g) denote linear fits to experimental data.

the MTJ films were microfabricated into nanopillar devices with a diameter of approximately 75 nm using electron-beam lithography and Ar-ion etching. The resistance-field (R-H) and differential conductance G were measured by connecting the device to a source measurement unit (Keysight B2902A) and a lock-in amplifier (Stanford Research Systems SR865), respectively. All magnetic and electrical measurements presented in this article were done at room temperature.

3. Results and discussion

3.1. Layer morphology, nanostructure and atomic distribution

Figures 1(a) and (b) show annular dark field (ADF) STEM images of MTJ films using MgO and MgFeO tunnel barriers, respectively. Both films were *ex-situ* annealed in a vacuum at a temperature T_a of 400°C for 1h. As expected from the poor wettability of CoFeB on MgO, the contrast at the MgO/CoFeB interface is blurred for the MgO-MTJ. Meanwhile, the ADF-TEM image taken of the MgFeO-MTJ reveals the formation of a flat MgFeO/CoFeB interface. The EDS elemental mapping shown in Figs. 1(c) and (d) also reveal improved flatness of the CoFeB free layer in the MgFeO-MTJ. Figure 1(e) shows the magnetization curves of MTJ films obtained under an out-of-plane H. After the annealing at $T_a = 400$°C, both MTJs exhibit perpendicular magnetization. Interestingly, we found that the use of MgFeO barrier not only affects the PMA in the free layer but also alters the magnetic stability of the reference layer coupled with the CoPt/Ir-based SAF layer. The possible origin of improved magnetic properties of reference layer and CoPt/Ir-based SAF layer will be discussed in detail in a later section. Figure 1(f) shows the minor magnetization curves of the MgFeO-MTJ films with different total CoFeB layer thickness t_{total}. Here, t_{total} corresponds to the thickness of the CoFeB/Mo/CoFeB free layer excluding the Mo layer thickness. For this thickness range, the CoFeB/Mo/CoFeB free layer exhibits distinct PMA and the magnetization direction can be sharply switched by applying a small magnetic field. The coercivity slightly increases with decreasing t_{total}, which can be attributed to an increase in the effective PMA energy density, K_{eff}, as will be revealed later by the FMR measurement. Figure 1(g) shows the saturation magnetization ($\mu_0 M_s t$) of the CoFeB/Mo/CoFeB free layer obtained from the minor magnetization curves as a function of t_{total}. For $t_{total} \geq 1.4$ nm, the $\mu_0 M_s t$ value almost linearly increases with increasing t_{total} for both the MgFeO- and MgO-MTJs, and the linear fit to the experimental data gives a dead layer thickness, $t_{dead} = 0.34$ nm (0.39 nm), as well as $\mu_0 M_s = 2.03$ (T) (1.97 T) for the MgFeO-MTJ (MgO-MTJ). The formation of

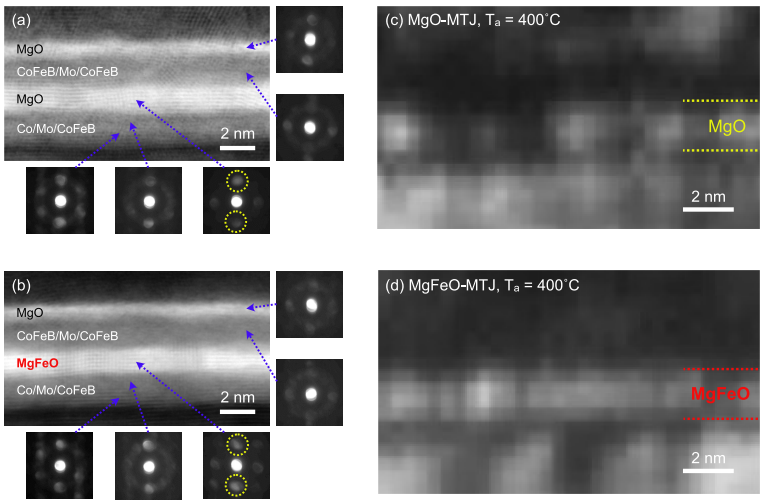

Figure 2: Nanostructural analysis on the MTJ films: (a, b) High-resolution BF-STEM images and NBD patterns for each layer, and (c, d) Virtual ADF-STEM images using the selected (002) and (00$\bar{2}$) diffraction spots as indicated by the dotted circles (a) and (b).

dead layer can be explained by the intermixing of CoFeB and Mo as well as the oxidation of CoFeB surface during the deposition of MgO capping layer. The slight reduction in t_{dead} in the MgFeO-MTJ is attributed to the segregation of ferromagnetic Fe from the MgFeO barrier associated with annealing [36].

Figures 2(a) and (b) show high-resolution bright field (BF) STEM images along with NBD patterns obtained from the MgO- and MgFeO-MTJs annealed at 400°C, respectively. In accordance with previous studies [39, 3, 40], the BF-STEM images as well as the NBD patterns reveal the formation of (001)-oriented MgO and MgFeO layers, and the CoFeB layers crystallize from the Mg(Fe)O/CoFeB interface. To compare the crystallinity of the Mg(Fe)O layer, virtual ADF-STEM images [41] are reconstructed using only the selected (002) and (00$\bar{2}$) diffraction spots as indicated by the dotted circles in Figs. 2(a) and (b) and shown in Figs. 2(c) and (d). The contrast of these images represents the diffraction intensity at the selected regions in the NBD patterns, i.e., the brighter areas contain a larger crystalline component having the same crystalline plane. In the MgO-MTJ, although a definite (001) orientation of MgO layer is observed

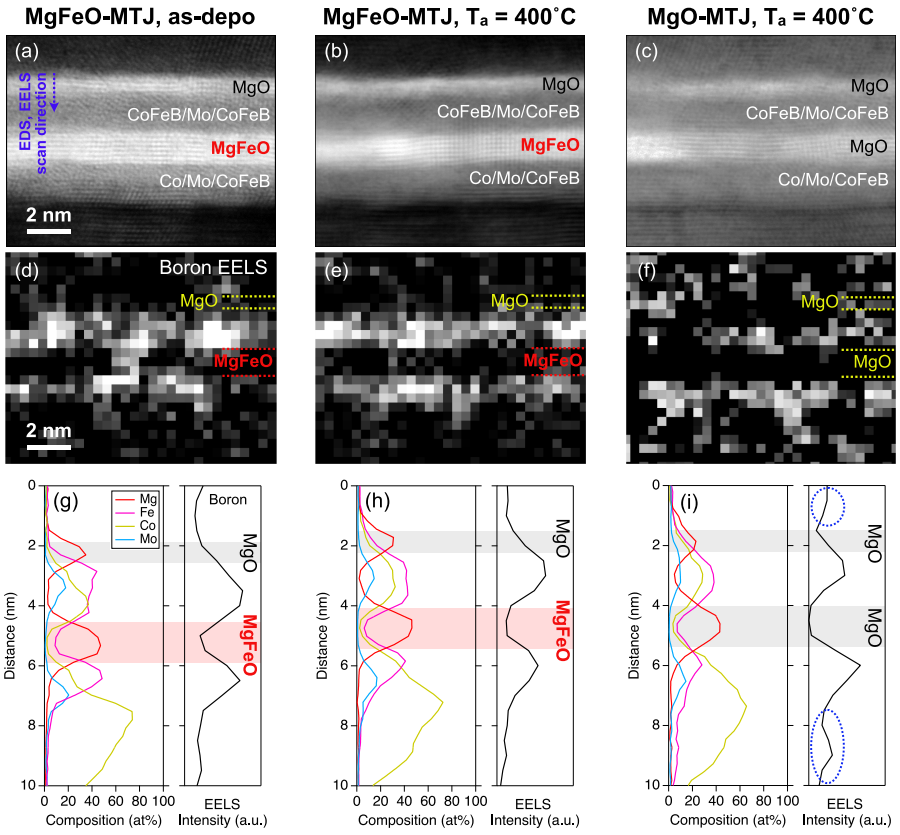

Figure 3: Cross-sectional images of MTJ films and compositional analyses: (a-c) BF-STEM images (d-e) EELS maps showing the distribution of B atoms. (g-f) Compositional line profiles obtained from the EDS and EELS analyses.

in both the BF-STEM image and the NBD patterns, the crystalline plane is found to be non-uniform over the film plane and thus contains many grain boundaries. In contrast, the reconstructed MgFeO layer is almost continuous along the film plane, which indicates good in-plane crystalline uniformity of the MgFeO tunnel barrier layer.

Figures 3(a)-(c) show BF-STEM images of as-deposited MgFeO-MTJ, MgFeO-MTJ annealed at 400°C, and MgO-MTJ annealed at 400°C, respectively, and Figs. 3(d)-(f) illustrate the distribution of B atoms in the corresponding area obtained from the EELS analysis. As shown in Fig. 3(a), the MgFeO layer

exhibits good crystallinity even in the as-deposited film, which can effectively eliminate the atomic diffusion from the CoFeB layer. In fact, the EELS maps shown in Figs. 3(d) and (e) reveal that the B atoms in the as-deposited CoFeB layers are confined in the CoFeB layers even after the annealing at 400°C. In the MgO-MTJ, however, the B atoms are dispersed from the CoFeB layer into the SAF and the capping layers, which suggests the diffusion of B atoms through the grain boundaries in the MgO layers. The integrated EELS intensities are shown in Figs. 3(g)-(i) together with compositional line profiles obtained from the EDS analysis. In the MgFeO-MTJ, the B atoms move away slightly from the MgFeO/CoFeB interface after annealing at 400°C associated with the crystallization of CoFeB to CoFe, but most B atoms remain in the CoFeB layers. In the MgO-MTJ annealed at 400°C, the EELS intensity at the CoFeB/Mo/CoFeB free layer is relatively weak and there are small peaks in the CoPt layer as well as the capping layer as denoted by the dotted circles in Fig. 3(i). Thus, the degraded magnetic property of SAF in the MgO-MTJ as observed in Fig. 1(e) can be explained by the diffusion of B atoms to the CoPt layer associated with annealing. The EDS line profiles also reveal the segregation of Fe from the MgFeO layer after the annealing; in the as-deposited MgFeO-MTJ, about 9 at% Fe is found in the MgFeO layer, whereas the Fe content is reduced to below 5 at% in the annealed MgFeO-MTJ and the diffused Fe atoms concentrate at the MgFeO/CoFeB interfaces. As a result, the MgFeO/CoFeB interfaces become Fe-rich compared with MgO/CoFeB interfaces in the MgO-MTJ. It is noteworthy that the atomic distributions in the CoFeB/Mo/CoFeB/MgO multilayer on the MgFeO layer are narrow and the transitions at the interfaces are sharper than those in the MgO-MTJ, which verifies the improved free layer flatness in the MgFeO-MTJ.

3.2. Magnetic anisotropy and magnetic damping of free layer

Figure 4(a) shows FMR spectra obtained from the MTJ films under an out-of-plane H. These spectra were obtained by sweeping H under a constant rf excitation at a frequency f of 35 GHz. The total CoFeB thickness t_{total} is 1.5

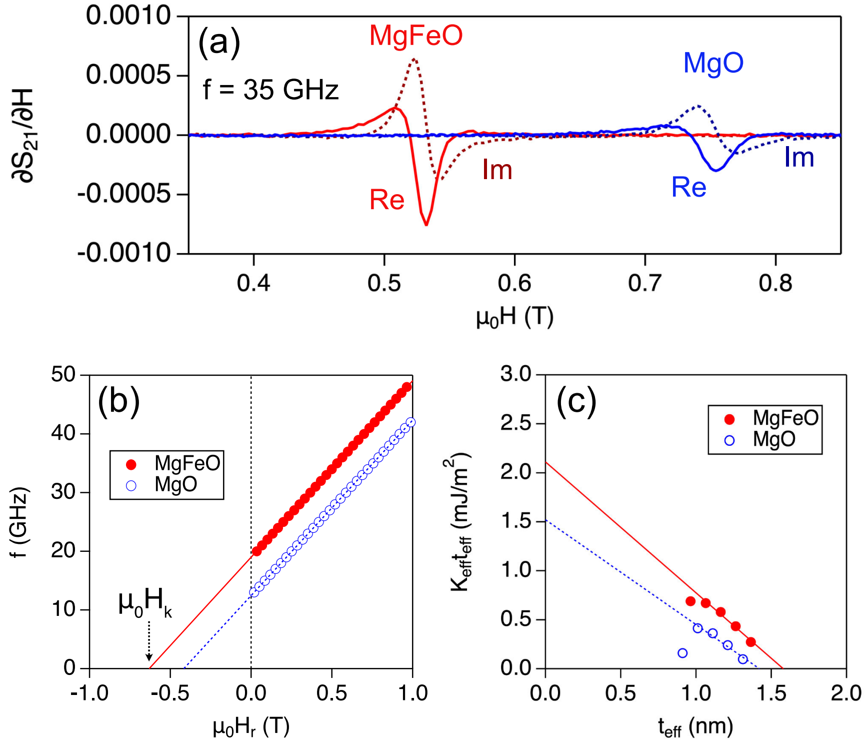

Figure 4: Results of FMR measurements: (a) FMR spectra obtained from the MTJ films under an out-of-plane H with f = 35 GHz, (b) Relationship between H_r and f. (c) $K_\mathrm{eff}t_\mathrm{eff}$ as a function of t_eff. Lines in (b) and (c) denote linear fits to the experimental data.

nm and the films were annealed at 400°C. For the same t_total, the free layer of the MgFeO-MTJ exhibits a narrower resonance linewidth ΔH and a larger resonance signal than that of the MgO-MTJ, suggesting a larger magnetization and a smaller magnetic damping in the MgFeO-MTJ. We also found that the resonance field (H_r) of the free layer in the MgFeO-MTJ is higher than that of MgO-MTJ under the same f. The relationship between H_r and f is shown in Fig. 4(b). For both MTJs, there is a linear relationship between H_r and f, and the anisotropy field H_k of the free layers are obtained from linear fits to the experimental data:

$$f = \frac{g\mu_0\mu_\mathrm{B}}{h}(H_\mathrm{r} - H_\mathrm{k}), \quad (1)$$

where h is Planck's constant, g is the Lande g-factor, and $\mu_{\rm B}$ is the Bohr magneton. Then, the areal PMA energy density $K_{\rm eff}t_{\rm eff}$ ($t_{\rm eff} = t_{\rm total} - t_{\rm dead}$) is estimated by using the obtained $H_{\rm k}$ values: $K_{\rm eff}t_{\rm eff} = M_{\rm s}H_{\rm k}/2$. Figure 4(c) shows the obtained $K_{\rm eff}t_{\rm eff}$ values as a function of $t_{\rm eff}$ for both MTJ films. The MgFeO-MTJs exhibit larger $K_{\rm eff}t_{\rm eff}$ than MgO-MTJs regardless of $t_{\rm eff}$, and a maximum $K_{\rm eff}t_{\rm eff}$ of 0.69 (0.41) mJ/m^2 is obtained at $t_{\rm eff} = 0.96$ (1.0) nm for the MgFeO-MTJs (MgO-MTJs). In addition, the y-intercept of the dependence of $K_{\rm eff}t_{\rm eff}$ on $t_{\rm eff}$ yields an estimated interfacial magnetic anisotropy energy density, $K_{\rm i}$, of 2.1 and 1.5 mJ/m^2 for the MgFeO- and MgO-MTJs, respectively. The enhanced interfacial PMA in the MgFeO-MTJ is attributed to the improved free layer flatness as well as the formation of Fe-rich region at the MgFeO/CoFeB interface [27].

Figures 5(a) and (b) show the FMR linewidth ΔH of the free layer as a function f for the MgFeO- and MgO-MTJs, respectively. For the both films, ΔH increases as $t_{\rm total}$ is reduced. To investigate the origin of increased ΔH in detail, we applied linear fitting to the experimental data [42]:

$$\Delta H = \frac{2h\alpha_{\rm total}}{g\mu_0\mu_{\rm B}} f + \Delta H_0, \tag{2}$$

where ΔH_0 is the inhomogeneous linewidth originating from the structural and/or magnetic inhomogeneities in the free layer. $\alpha_{\rm total}$ corresponds to the total magnetic damping which includes the radiative damping [43] and the interfacial enhancement of damping due to the spin pumping effect [44, 45, 42]. However, we neglect the radiative damping in the following discussion since its contribution can be ignored for ultrathin films. Note that we also omit the data obtained from the MgO-MTJ with $t_{\rm total} = 1.3$ nm, because there is an anomalous enhancement of ΔH for $t_{\rm total} = 1.3$ nm as shown in the inset of Fig. 5(b), which may originate from discontinuity in the free layer.

The ΔH_0 and $\alpha_{\rm total}$ values obtained from the fitting to the experimental data using Eq. (1) are shown in Fig. 5(c) and (d), respectively. For the same $t_{\rm eff}$, the MgFeO-MTJ exhibits a smaller ΔH_0 compared with the MgO-MTJ. The reduced ΔH_0 in the MgFeO-MTJ can be attributed to the improved flatness

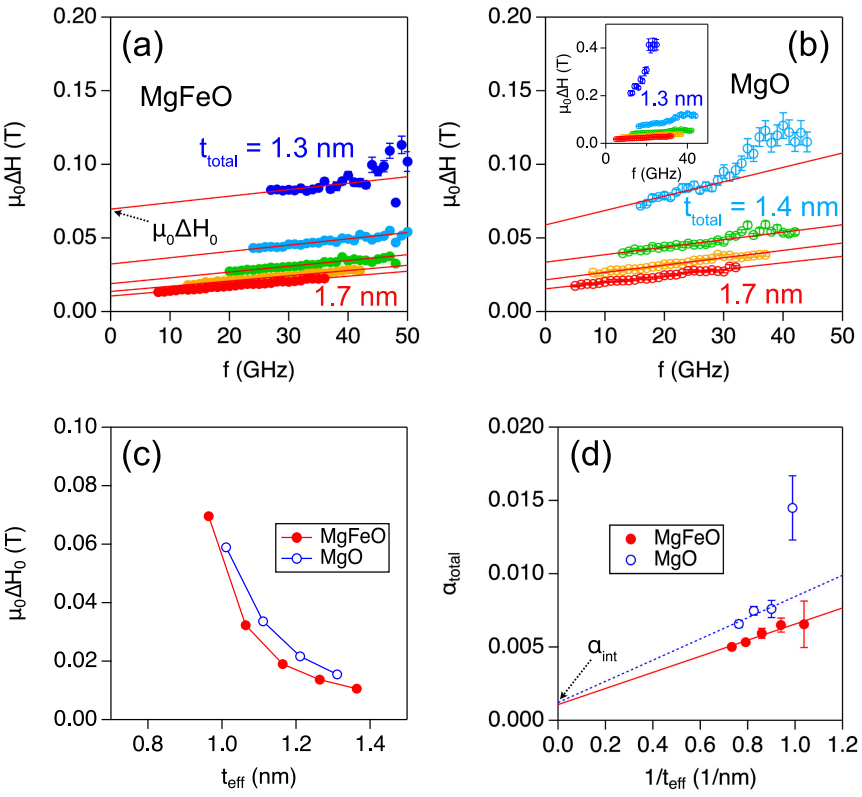

Figure 5: FMR linewidth and magnetic damping of free layers with various t_{total}: (a, b) ΔH as a function of f, (c) ΔH_0 as a function of t_{eff}, and (d) α_{total} as a function of $1/t_{\mathrm{eff}}$. Lines in (d) denote linear fits to the experimental data.

of the free layer as determined by the TEM-EDS analyses. As is the case with ΔH_0, α_{total} increases with decreasing t_{eff}. The dependence of α_{total} on $1/t_{\mathrm{eff}}$ is shown in Fig. 5(d). The y-intercept corresponds to the intrinsic magnetic damping, α_{int}, which is free of the spin pumping effect and the value should be the same for ferromagnets with the same composition and crystal structure. The obtained α_{int} values, $\alpha_{\mathrm{int}} = 0.0055$ for the MgFeO-MTJ and $\alpha_{\mathrm{int}} = 0.0072$ for the MgO-MTJ, are in agreement with those reported for FeCo alloy thin films [42], while the shallower slope of α_{total} on $1/t_{\mathrm{eff}}$ for the MgFeO-MTJ suggests a reduced magnon scattering owing to the improved film uniformity and/or

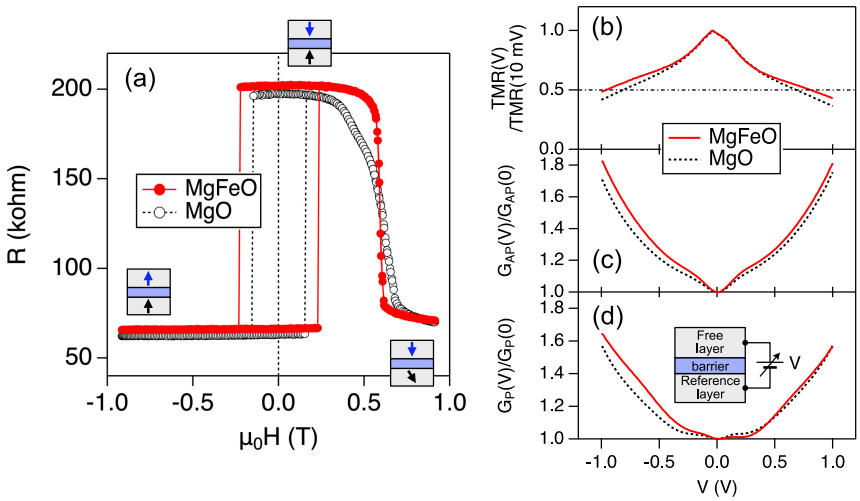

Figure 6: Magneto-transport properties of MTJ nanopillar devices: (a) *R-H* curves measured under an out-of-plane H with $V = 10$ mV. (b-d) V dependence of (b) TMR(V)/TMR(10 mV), (c) $G_{\rm AP}(V)/G_{\rm AP}(0)$, and (d) $G_{\rm P}(V)/G_{\rm P}(0)$. $t_{\rm total} = 1.5$ nm for both devices.

reduced atomic interdiffusion.

3.3. Magneto-transport properties of MTJ nanopillars

Finally, we discuss the magneto-transport properties of nanopillar MTJ devices. Figure 6(a) shows *R-H* curves of MgFeO- (filled circles) and MgO-MTJ devices (open circles) measured under a perpendicular H and a dc bias voltage V of 10 mV. The total free layer thickness $t_{\rm total} = 1.5$ nm. The MTJ films were annealed at $T_{\rm a} = 400°$C for 1h prior to the microfabrication. Both MTJ devices exhibit sharp changes in resistance at around $\mu_0 H = \pm 0.2$ T associated with the switching of free layer magnetization, where the high- and low-resistance state corresponds to the antiparallel (AP) and parallel (P) alignment of the free layer and the reference layer magnetizations, respectively. The two MTJ devices exhibit similar AP and P resistances, and TMR ratios of around 200% are obtained for both devices. In accordance with the VSM and VNA-FMR measurement results, the MgFeO-MTJ device exhibits a higher magnetic stability than the MgO-MTJ devices, i.e., the free layer exhibits a larger coercivity and

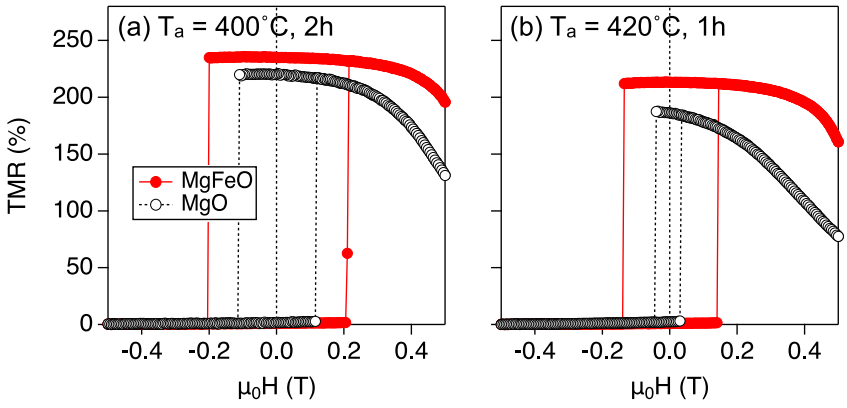

Figure 7: TMR curves of MTJ nanopillar devices microfabricated from MTJ films annealed at different conditions: (a) $T_{\rm a} = 400$°C for 2h and (b) $T_{\rm a} = 420$°C for 1h. $t_{\rm total} = 1.5$ nm for all devices.

the reference layer maintains a flat and a broader plateau for the AP state.

Figures 6(b)-(d) show the V dependence of the TMR ratio and differential conductances under the AP ($G_{\rm AP}$) and P ($G_{\rm P}$) states, respectively. The values of the TMR ratio and differential conductances are divided by the values at $V = 10$ mV and 0 mV, respectively. The use of the MgFeO tunnel barrier alters the symmetry of conductance curve for the P state, and the deviation from parabolic curve at the low V region becomes more visible. These results are indicative of the enhanced contribution of tunneling conductance specific to crystalline CoFe/MgO/CoFe MTJs with clean interfaces [46] in the MgFeO-MTJ. It is also shown that the use of the MgFeO tunnel barrier weakens the dependence of the TMR ratio on V. The V range for which the MTJ retains TMR(V)/TMR(10 mV) > 0.5 is enhanced from -0.80 V $\leq V \leq 0.65$ V to -0.94 V $\leq V \leq 0.79$ V by replacing the MgO tunnel barrier with the MgFeO one. The overall improvements in the magnetic and electrical transport properties in the MgFeO-MTJ would be worth exploring in terms of practical applications.

To further investigate the tolerance of MTJs against high-$T_{\rm a}$ annealing, we prepared two sets of MTJ nanopillar devices, one annealed at $T_{\rm a} = 400$°C for

2h [Fig. 7(a)] and the other annealed at $T_a = 420°C$ for 1h [Fig. 7(b)] prior to the microfabrication. The total free layer thickness $t_{total} = 1.5$ nm. After the annealing at $T_a = 400°C$ for 2h, the TMR ratio of MgFeO-MTJ is enhanced by up to 235%. Although the TMR ratio of the MgO-MTJ is not affected by the longer annealing time, the reduction in the coercivity and the plateau region for the AP state indicate the degradation of PMA in both the free layer and the reference layer. The degradation of PMA is greater for the MgO-MTJ annealed at $T_a = 420°C$ for 1h; the coercivity is reduced to as low as 0.05 T, and the AP magnetization configuration is incomplete at $H = 0$ T. Meanwhile, the MgFeO-MTJ exhibits coercivity as large as 0.15 T, and the plateau of the AP state extends up to ~ 0.3 T even after the annealing at $T_a = 420°C$. These experimental results clearly demonstrate that the MgFeO-MTJ is tolerant of a higher T_a for a longer duration.

4. Conclusions

We have evaluated the magnetic and electrical transport properties of MTJs using MgO and MgFeO tunnel barriers. The use of MgFeO barrier substantially improved the flatness of the free layer owing to the improved wettability of CoFeB, and $K_{eff}t_{eff}$ is enhanced by a factor of 1.7 compared with that of MgO-MTJ. At the same time, the improved homogeneity in the free layer contributed to reducing $\mu_0\Delta H_0$ and α_{total}. Detailed nanostructural analysis revealed the uniform (001)-oriented growth of MgFeO barrier layer, which effectively inhibited the segregation of B atoms from the CoFeB layers during the high-temperature annealing process. The improved thermal tolerance in the MgFeO-MTJ makes it possible to attain a large TMR ratio of 235% after the annealing at $T_a = 400°C$ for 2h. These experimental demonstrations should be beneficial for the development of high-density and energy-efficient MRAMs.

Acknowledgement

The authors would like to thank T. Nozaki, M. Konoto, A. Sugihara, S. Tsunegi, Y. Hibino, L. Sakai, K. Ohba, H. Ohmori, Y. Higo, Y. Kageyama and M. Hosomi for their fruitful discussions, and M. Toyoda, and K. Suzuki for assisting with the experiments. This work is based on results obtained from a project, JPNP16007, commissioned by the New Energy and Industrial Technology Development Organization (NEDO), Japan.

References

[1] S. S. P. Parkin, C. Kaiser, A. Panchula, P. M. Rice, B. Hughes, M. Samant, S.-H. Yang, Giant tunneling magnetoresistance at room tempereature with MgO (100) tunnel barriers, Nat. Mater. 3 (2004) 862.

[2] S. Yuasa, T. Nagahama, A. Fukushima, Y. Suzuki, K. Ando, Giant room-temperature magnetoresistance in single-crystal Fe/MgO/Fe magnetic tunnel junctions, Nat. Mater. 3 (2004) 868.

[3] D. Djayaprawira, K. Tsunekawa, M. Nagai, H. Maehara, S. Yamagata, N. Watanabe, S. Yuasa, Y. Suzuki, K. Ando, 230% room-temperature magnetoresistance in CoFeB/MgO/CoFeB magnetic tunnel junctions, Appl. Phys. Lett. 86 (2005) 092502.

[4] J. Mathon, A. Umerski, Theory of tunneling magnetoresistance of an epitaxial Fe/MgO/Fe (001) junction, Phys. Rev. B 63 (2001) 220403.

[5] W. H. Butler, X.-G. Zhang, T. C. Schulthess, J. M. MacLaren, Spin-dependent tunneling conductance of Fe—MgO—Fe sandwiches, Phys. Rev. B 63 (2001) 054416.

[6] S. Yakata, H. Kubota, Y. Suzuki, K. Yakushiji, A. Fukushima, S. Yuasa, K. Ando, Influence of perpendicular magnetic anisotropy on spin-transfer switching current in CoFeB/MgO/CoFeB magnetic tunnel junctions, J. Appl. Phys. 105 (2009) 07D131.

[7] D. Worledge, G. Hu, D. W. Abraham, P. Trouilloud, S. Brown, Development of perpendicularly magnetized Ta—CoFeB—MgO-based tunnel junctions at ibm, J. Appl. Phys. 115 (2014) 172601.

[8] S. Ikeda, K. Miura, H. Yamamoto, K. Mizunuma, H. D. Gan, M. Endo, S. Kanai, J. Hayakawa, F. Matsukura, H. Ohno, A perpendicular-anisotropy CoFeB-MgO magnetic tunnel junction, Nat. Mater. 9 (2010) 721.

[9] T. Shinjo, S. Hine, T. Takada, Mössbauer spectra of ultrathin Fe films coated by MgO, J. de Phys. 40 (1979) C2–86.

[10] H. Kubota, S. Ishibashi, T. Saruya, T. Nozaki, A. Fukushima, K. Yakushiji, K. Ando, Y. Suzuki, S. Yuasa, Enhancement of perpendicular magnetic anisotropy in FeB free layers using a thin MgO cap layer, J. Appl. Phys. 111 (2012) 07C723.

[11] H. X. Yang, M. Chshiev, B. Dieny, J. H. Lee, A. Manchon, K. H. Shin, First-principles investigation of the very large perpendicular magnetic anisotropy at Fe—MgO and Co—MgO interfaces, Phys. Rev. B 84 (2011) 054401.

[12] J. Okabayashi, J. W. Koo, H. Sukegawa, S. Mitani, Y. Takagi, T. Yokoyama, Perpendicular magnetic anisotropy at the interface between ultrathin Fe film and MgO studied by angular-dependent X-ray magnetic circular dichroism, Appl. Phys. Lett. 105 (2014) 122408.

[13] H. Yoda, T. Kishi, T. Nagase, M. Yoshikawa, K. Nishimata, E. Kitagawa, T. Daibou, M. Amano, N. Shimomura, S. Takahashi, T. Kai, M. Nakayama, H. Aikawa, S. Ikegawa, M. Nagamine, J. Ozeki, S. Mizukami, M. Oogane, Y. Ando, S. Yuasa, K. Yakushiji, H. Kubota, Y. Suzuki, Y. Nakatani, T. Miyazaki, K. Ando, High efficient spin transfer torque writing on perpendicular magnetic tunnel junctions for high density mrams, Curr. Appl. Phys. 10 (2010) e87.

[14] K. Ando, S. Fujita, J. Ito, S. Yuasa, Y. Suzuki, Y. Nakatani, T. Miyazaki, H. Yoda, Spin-transfer torque magnetoresistive random-access memory technologies for normally off computing, J. Appl. Phys. 115 (2014) 172607.

[15] L. Thomas, G. Jan, J. Zhu, H. Liu, Y.-J. Lee, S. Le, R.-Y. Tong, K. Pi, Y.-J. Wang, D. Shen, R. He, J. Haq, J. Teng, V. Lam, K. Huang, T. Zhong, T. Torng, P.-K. Wang, Perpendicular spin transfer torque magnetic random access memories with high spin torque efficiency and thermal stability for embedded applications, J. Appl. Phys. 115 (2014) 172615.

[16] B. Dieny, M. Chshiev, Perpendicular magnetic anisotropy at transition metal/oxide interfaces and applications, Rev. Mod. Phys. 89 (2017) 025008.

[17] C. Chappert, A. Fert, F. Dau, The emergence of spin electronics in data storage, Nat. Mater. 6 (2007) 813.

[18] K. Yakushiji, T. Saruya, H. Kubota, A. Fukushima, T. Nagahama, S. Yuasa, K. Ando, Ultrathin Co/Pt amd Co/Pt superlattice films for MgO-based perpendicular magnetic tunnel junctions, Appl. Phys. Lett. 97 (2010) 232508.

[19] K. Yakushiji, A. Sugihara, A. Fukushima, H. Kubota, S. Yuasa, Very strong antiferromagnetic interlayer exchange coupling with iridium spacer layer for perpendicular magnetic tunnel junctions, Appl. Phys. Lett. 110 (2017) 092406.

[20] H. Sato, M. Yamanouchi, S. Ikeda, S. Fukami, F. Matsukura, H. Ohno, Perpendicular-anisotropy CoFeB-MgO magnetic tunnel junctions with a MgO/CoFeB/Ta/CoFeB/MgO recording structure, Appl. Phys. Lett. 101 (2012) 022414.

[21] J.-H. Kim, J.-B. Lee, G.-G. An, S.-M. Yang, W.-S. Chung, H.-S. Park, J.-P. Hong, Ultrathin W space layer-enabled thermal stability enhancement in a perpendicular MgO/CoFeB/W/CoFeB/MgO recording frame, Sci. Rep. 5 (2015) 16903.

[22] S. Miura, T. Nguyen, Y. Endo, H. Sato, S. Ikeda, K. Nishioka, H. Honjo, T. Endoh, Insertion layer thickness dependence of magnetic and electrical properties for double-CoFeB/MgO-interface magnetic tunnel junctions, IEEE Trans. Magn. 55 (2019) 3401004.

[23] H. Cheng, J. Chen, S. Peng, B. Zhang, Z. Wang, D. Zhu, K. Shi, S. Eimer, X. Wang, Z. Guo, Y. Xu, D. Xiong, K. Cao, W. Zhao, Giant perpendicular magnetic anisotropy in Mo-based double-interface free layer structure for advanced magnetic tunnel junctions, Adv. Electron. Mater. 6 (2020) 2000271.

[24] D.-Y. Lee, S.-H. Hong, S.-E. Lee, J.-G. Park, Material for double MgO based perpendicular-magnetic-tunneling-junction, Sci. Rep. 6 (2016) 38125.

[25] M. Wang, W. Cai, K. Cao, J. Zhou, J. Wrona, S. Peng, H. Wei, W. Kang, Y. Zhang, J. Langer, B. Ocker, A. Fert, W. Zhao, Current-induced magnetization switching in atom- thick tungsten engineered perpendicular magnetic tunnel junctions with large tunnel magnetoresistance, Nat. Commun. 9 (2018) 671.

[26] S. Couet, T. Devolder, J. Swerts, S. Mertens, T. Lin, E. Liu, S. Elshocht, G. Kar, Impact of Ta and W-based spacers in double MgO STT-MRAM free layers on perpendicular anisotropy and damping, Appl. Phys. Lett. 111 (2017) 152406.

[27] T. Yamamoto, T. Nozaki, K. Yakushiji, S. Tamaru, H. Kubota, A. Fukushima, S. Yuasa, Perpendicular magnetic anisotropy and its voltage control in MgO/CoFeB/MgO junctions with atomically thin Ta adhesion layers, Acta. Mater. 216 (2021) 117097.

[28] T. Maruyama, Y. Shiota, T. Nozaki, K. Ohta, N. Toda, M. Mizuguchi, A. A. Tulapurkar, T. Shinjo, M. Shiraishi, S. Mizukami, Y. Ando, Y. Suzuki, Large voltage-induced magnetic anisotropy change in a few atomic layers of iron, Nat. Nanotech. 4 (2009) 158.

[29] Y. Shiota, T. Nozaki, F. Bonell, S. Murakami, T. Shinjo, Y. Suzuki, Induction of coherent magnetization switching in a few atomic layers of FeCo using voltage pulses, Nat. Mater. 11 (2012) 39.

[30] S. Kanai, M. Yamanouchi, S. Ikeda, Y. Nakatani, F. Matsukura, H. Ohno, Electric field-induced magnetization reversal in a perpendicular-anisotropy CoFeB-MgO magnetic tunnel junction, Appl. Phys. Lett. 101 (2012) 122403.

[31] P. K. Amiri, J. G. Alzate, X. Q. Cai, F. Ebrahimi, Q. Hu, K. Wong, C. Grezes, H. Lee, G. Yu, X. Li, M. Akyol, Q. S. J. A. Katine, J. Langer, B. Ocker, K. L. Wang, Electric-field-controlled magnetoelectric RAM: progress, challenges, and scaling, IEEE Trans. Magn. 51 (2015) 3401507.

[32] T. Yamamoto, R. Matsumoto, T. Nozaki, H. Imamura, S. Yuasa, Developments in voltage-controlled subnanosecond magnetization switching, J. Magn. Magn. Mater. 560 (2022) 169637.

[33] T. Ichinose, T. Yamamoto, T. Nozaki, K. Yakushiji, S. Tamaru, M. Konoto, S. Yuasa, Cryogenic temperature deposition of high-performance CoFeB/MgO/CoFeB magnetic tunnel junctions on ϕ300 mm wafers, ACS Appl. Electron. Mater. 5 (2023) 2178.

[34] A. Sugihara, T. Ichinose, S. Tamaru, T. Yamamoto, M. Konoto, T. Nozaki, S. Yuasa, Low magnetic damping in an ultrathin cofeb layer deposited on a 300 mm diameter wafer at cryogenic temperature, Appl. Phys. Express 16 (2023) 023003.

[35] T. Nozaki, T. Ohkubo, Y. Shiota, H. Kubota, A. Fukushima, K. Hono, Y. Suzuki, S. Yuasa, Growth of a high-quality ultrathin Fe(001) layer on MgO(001) by insertion of an ultrathin γ-Fe_2O_3 layer, Appl. Phys. Express 4 (2011) 113004.

[36] K. Yakushiji, E. Kitagawa, T. Ochiai, H. Kubota, N. Shimomura, J. Ito, H. Yoda, S. Yuasa, Fabrication of Mg-X-O (X = Fe, Co, Ni, Cr, Mn, Ti,

V, and Zn) barriers for magnetic tunnel junctions, AIP Advances 8 (2018) 055905.

[37] T. Ichinose, T. Yamamoto, T. Nozaki, K. Yakushiji, S. Tamaru, S. Yuasa, Interfacial Fe segregation and its influence on magnetic properties of CoFeB/MgFeO multilayers, arXiv (2023) 2308.08876.

[38] S. Tamaru, T. Yamamoto, T. Onuma, N. Kikuchi, S. Okamoto, Development of a high-sensitivity VNA-FMR spectrometer with field modulation detection and its application to magnetic characterization, Electron. Comm. Jpn 104 (2021) e12320.

[39] C. Wang, K. Do, M. Beasley, T. Geballe, R. Hammond, Deposition of in-plane textured mgo on amorphous Si_3N_4 substrates by ion-beam-assisted deposition and comparisons with ion-beam-assisted deposited yttria-stabilized-zirconia, Appl. Phys. Lett. 71 (1997) 2995.

[40] S. Yuasa, Y. Suzuki, T. Katayama, K. Ando, Characterization of growth and crystallization processes in CoFeB/MgO/CoFeB magnetic tunnel junction structure by reflective high-energy electron diffraction, Appl. Phys. Lett. 87 (2005) 242503.

[41] C. Gammer, V. Ozdol, C. Liebscher, A. Minor, Diffraction contrast imaging using virtual apertures, Ultramicroscopy 155 (2015) 1.

[42] M. Schoen, D. Thonig, M. Schneider, T. Silva, H. Nembach, O. Eriksson, O. Karis, J. Shaw, Ultra-low magnetic damping of a metallic ferromagnet, Nat. Phys. 12 (2016) 839.

[43] M. Schoen, J. Shaw, H. Nembach, M. Weiler, T. Silva, Radiative damping in waveguide-based ferromagnetic resonance measured via analysis of perpendicular standing spin waves in sputtered permalloy films, Phys. Rev. B 92 (2015) 184417.

[44] S. Mizukami, Y. Ando, T. Miyazaki, The study on ferromagnetic resonance linewidth for NM/80NiFe/NM (NM = Cu, Ta, Pd and Pt) films, Jpn. J. Appl. Phys. 40 (2001) 580.

[45] Y. Tserkovnyak, A. Brataas, G. Bauer, Enhanced gilbert damping in thin ferromagnetic films, Phys. Rev. B 88 (2013) 117601.

[46] T. Scheike, Z. Wen, H. Sukegawa, S. Mitani, Enhanced tunnel magnetoresistance in Fe/Mg_4Al-O_x/Fe(001) magnetic tunel junctions, Appl. Phys. Lett. 120 (2022) 032404.